Applied Organometallic Chemistry

WILEY

Applied Organometallic Chemistry

RESEARCH ARTICLE OPEN ACCESS

Luminescent Sensing of 1,3,5-Trinitrotoluene Using a Schiff Base Ligand and Cd(II) Complex: Structural and Photophysical Investigations

Nevin Turan[1] | Ayhan Altun[2] | Kenan Buldurun[3] | Olcay Aydın[1]

[1]Department of Chemistry, Faculty of Arts and Sciences, Muş Alparslan University, Muş, Turkey | [2]Department of Chemistry, Gebze Technical University, Kocaeli, Turkey | [3]Department of Food Processing, Technical Science Vocational School, Muş Alparslan University, Muş, Turkey

Correspondence: Nevin Turan (n.turan@alparslan.edu.tr) | Ayhan Altun (altun@gtu.edu.tr)

Received: 31 March 2025 | **Revised:** 10 April 2025 | **Accepted:** 27 April 2025

Funding: This research was supported by the Muş Alparslan University Scientific Research Project Unit under project number BAP-22-FEF-4902-08.

Keywords: Cd(II) complex | fluorescence emission | NACs | Schiff base | spectroscopy | TNT

ABSTRACT

The Schiff base (H_2L) was synthesized by condensing 2-amino-6-methyl-4,5,6,7-tetrahydrothieno[2,3-*c*]pyridine-3-carboxamide with 5-bromo-2-hydroxybenzaldehyde in a 1:2 M ratio, yielding the product with high efficiency. This Schiff base then formed a coordination complex with Cd(II) in a 1:1 M ratio, resulting in the complex $[H_2LCd(H_2O)_2]\cdot 1.5H_2O$. The synthesis and structural characterization of H_2L and its Cd(II) complex were carried out using various techniques, including microanalysis (CHNS), FTIR, ^1H and ^{13}C-NMR, mass, UV–visible, magnetic susceptibility, thermogravimetric analysis (TGA), and fluorescence spectroscopy. The spectral data suggested that the Cd(II) complex adopted an octahedral geometry. In addition to the structural studies, the fluorescence properties of H_2L and its Cd(II) complex were investigated. Sensor properties of the Cd(II) complex for detecting nitroaromatic compounds were assessed using fluorescence spectroscopy. Both compounds exhibited high sensitivity for the detection of 1,3,5-trinitrotoluene (TNT). Specifically, H_2L demonstrated a low limit of detection (LOD) of 0.094 μM in the linear range of 1–10 μM. The fluorescence studies revealed that H_2L and its Cd(II) complex displayed strong fluorescence emissions. Furthermore, the Schiff base was employed for detecting TNT through fluorescence quenching, showing excellent selectivity and sensitivity.

1 | Introduction

In metal chemistry, Schiff coordination bases have been described as "privileged ligands," with applications in many industries and fields, including chemistry, organic synthesis, analytics, and optical and electrochemical sensors. Schiff base transition metal complexes also have applications in the food, leather, and wood dyeing industries. Schiff bases and Schiff base transition metal complexes have garnered significant attention in research owing to their distinctive coordination characteristics and the broad range of potential applications. Schiff base ligands enable the utilization of Schiff base metal complexes in various practical applications by coordinating with a wide range of metals and stabilizing them across different oxidation states [1–5]. Heterocyclic moieties, including N, O, or S atoms, are frequently found in Schiff bases. These atoms enhance the ligand's polarizability, improving its solubility in common organic solvents. Additionally, the functional diversity of these ligands allows for their use in a wide range of applications [6, 7]. The physical and chemical properties of these compounds can be modulated by the great versatility of the ligand structural modifications [8, 9]. Transition metals are extensively utilized in both industrial and nonindustrial processes, where they play a crucial role. Numerous chemical sensors have been developed due to the biological and environmental significance of

various metal ions. These sensors are simple, are highly selective, are sensitive, have low detection limits, and are cost-effective [10]. Among the various methods, fluorescence probes have become essential for detecting metal ions.

Nitroaromatic compounds (NACs) are important components of pharmaceuticals, insecticides, and explosives and play an important role in a variety of industrial processes [11–13]. These substances are highly toxic and carcinogenic, posing a threat to both human health and ecosystems [14–16]. There has been significant interest in developing sensitive and selective detection methods due to the known risks to life associated with current detection techniques. In particular, compounds such as TNT and TNP have raised concerns due to their use in explosives and their environmental effects [17], and the detection of even trace amounts of these is essential for environmental and public safety.

Due to military activities, the produced TNT has contaminated groundwater, soils, and natural water resources [18]. Intensive exposure to TNT has toxic effects on many organisms, such as humans, fungi, and plants. Therefore, contaminated areas should be identified, monitored, and eventually remediated. The permissible concentration of TNT in drinking water has been set by the US Environmental Protection Agency (USEPA) as 2 ppb (~8.8×10^{12} M) [19]. As a result, there is an urgent need to improve detection technologies for continuous monitoring in these harsh environments.

Typical techniques used for explosive detection encompass mass spectrometry [20], ion mobility spectrometry [21], gas chromatography [22], fluorescence spectroscopy [23, 24], colorimetric methods [25], electrochemical analysis [26], electrophoresis [27], and others. Fluorescence spectroscopy is particularly popular among these methods because of its high sensitivity, rapid response, excellent selectivity, and real-time and on-site analysis capabilities [28].

In recent years, the rational design and synthesis of metal–organic complexes have attracted significant attention due to their wide applications in various fields (e.g., electrochemistry, photoluminescence and ion exchange, various topological structures, and gas absorption and storage) [29]. The first section of this study involves the synthesis and structural characterization of a new Cd(II) complex and a H_2L, which is obtained from a carboxamide compound and 5-bromo-2-hydroxybenzaldehyde. The molecular structures of both H_2L and its Cd(II) complex were carefully examined using various spectral and analytical methods. The second section of this study is dedicated to investigating the photophysical properties of H_2L and its Cd(II) complex. It is well known that Schiff bases exhibit distinct fluorescent sensor properties.

2 | Experimental

2.1 | Materials and Instrumentation

$Cd(NO_3)_2{\cdot}4H_2O$, along with the starting materials for the ligand and the solvents or reagents used in this study, was obtained from Merck Chemical Company and was used as received, without any additional purification. Microanalysis was performed by a Thermo-Finnigan Flash EA 1112 Series Elementary Analyzer. FTIR spectra were obtained with a PerkinElmer 65 spectrometer in the range of 4000–400 cm^{-1}, with KBr as the sample medium. ^1H and ^{13}C-NMR spectra were recorded on a Bruker 300 Merkur spectrometer, operating at 300 MHz (^1H) and 75.47 MHz (^{13}C), using DMSO-d_6 as the solvent, with TMS as the internal standard. Magnetic susceptibility measurements were performed using the standard Gouy tube method, with $Hg[Co(SCN)_4]$ as the calibrate. Thermogravimetric analyses (TG-DTA) were conducted under nitrogen gas flow, ranging from 25°C to 1000°C, using a Shimadzu TGA-50H thermal analyzer. Mass spectra were obtained using an AB Sciex 3200 QTrap spectrometer. The melting points and decomposition temperatures were measured using a STUART SMP30 melting point apparatus. UV–Vis absorption experiments were carried out by a UV-1800 UV/Vis scanning spectrophotometer (Shimadzu, Japan). Fluorescence spectra were measured with a Cary Eclipse spectrofluorometer (Varian, United States). Time-resolved fluorescence measurements were conducted using a Fluorolog 3-2iHR spectrofluorometer, with a TCSPC module employed as the excitation source at 390 nm (Horiba Jobin-Yvon-SPEX, France).

2.2 | Synthesis of Schiff Base (H_2L)

The different amounts (1:2 M ratio) of the amine compound (0.50 g, 2.36 mmol) and 5-bromo-2-hydroxybenzaldehyde (0.95 g, 4.73 mmol) have to be refluxed in 15 mL of hot methyl alcohol for 2 h to prepare H_2L (Figure 1). The yellow precipitate of ligand was formed, separated by filtration, washed several times with methyl alcohol and diethyl ether, and dried at room temperature [30]. Yellow solid; yield: 85%; m. p.: 235°C; Anal. calc. for $C_{23}H_{19}Br_2N_3O_3S$ (577.12 g/mol): C, 47.86; H, 3.29; N, 7.28; S, 5.55%. Found: C, 47.88; H, 3.30; N, 7.27; S, 5.56%; FTIR (KBr, υ_{max}) cm^{-1}: 3426, 3350 (-OH), 3017 (Ar. -CH), 2979, 2941 (Aliph. -CH), 1689 (C=O), 1668, 1609 (CH=N), 1573, 1540, 1505 (Ar. C=C), 1204, 1188 (C-O), 667 (C-Br), 776 (C-S-C); ^1H-NMR (DMSO-d_6, δ, ppm): 9.48 (s, 2H, OH), 8.59 (s, 2H, CH=N), 7.57–6.62 (m, 6H, Ar. -CH), 3.73 (s, 2H, py), 2.74 (t, 4H, py), 2.27 (s, 3H, $-CH_3$) (Figure S1); ^{13}C-NMR (DMSO-d_6, δ, ppm): 169.78 (C=O), 162.34, 159.95 (CH=N), 157.69–112.20 (benzene and thiophene), 58.94–44.99 (py), 23.34 ($-CH_3$) (Figure S2); Electronic spectra (λmax, nm, ε (L/mol cm): 197 (3427), 201 (4534), 210 (3647), 225 (10000), 285 (1318); 340 (1497), 368 (1829), 395 (2062).

2.3 | Synthesis of the Cd(II) Complex

$H_2LCd(H_2O)_2]1{\cdot}5H_2O$ was synthesized by refluxing one equivalent of H_2L (0.60 g, 1.04 mmol) with one equivalent of $Cd(NO_3)_2{\cdot}4H_2O$ (0.32 g, 1.04 mmol) in methanol overnight. The solid product was filtered, extensively washed with hot methanol, and subsequently dried at room temperature. The proposed structure formula for the Cd(II) complex is given in Figure 1 [30]. Dark red solid; yield: 70%; m. p.: 270°C; anal calc. for $C_{23}H_{24}Br_2N_3O_{6.5}SCd$ (750.53 g/mol): C, 36.80; H, 2.53; N, 5.60; S, 4.27%. Found: C, 36.81; H, 2.55; N, 5.58; S, 4.28%; ^1H-NMR (DMSO-d_6, δ, ppm): 8.94 (s, 2H, CH=N), 8.00–7.18 (m, 6H, Ar. -CH), 3.91 (s, 2H, py), 3.01–2.73 (t, 4H, py), 2.28 (s, 3H, $-CH_3$) (Figure S3); ^{13}C-NMR (DMSO-d_6, δ, ppm): 172.99 (C=O), 165.23 (CH=N), 158.42–110.47 (benzene and thiophene ring),

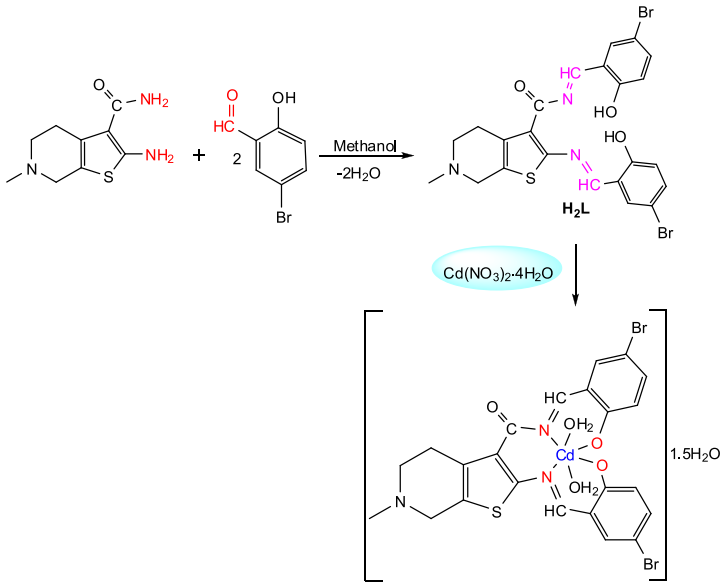

FIGURE 1 | Synthetic route of H_2L and its Cd(II) complex.

59.08–44.99 (py), 23.34 (-CH_3) (Figure S4); FTIR (KBr, υ max (cm^{-1})): 3418 $(OH/H_2O)_{br}$, 3115, 3028 (Ar. -CH), 2952, 2914 (Aliph. -CH), 1677 $(C=O)_{br}$, 1641, 1618 (CH=N), 1596, 1556, 1531, 1507 (Ar. C=C), 1238, 1181 (C-O), 829 (H_2O), 779 (C-S-C), 555, 535, 508 (Cd-O), 493, 484, 461 (Cd-N); electronic spectra (λmax, nm, ε (L/mol cm): 205 (3352), 215 (3866), 226 (3808), 239 (3391), 247 (2883), 267 (1649); 320 (373), 340 (405), 365 (325), 410 (521), 715 (4); mass spectrum (ESI): *m/z* 752.530 (calc.), 752.226 (found) $[M+2H]^{2+}$.

2.4 | Photophysical Measurements

The absorption and luminescence spectra of new H_2L and its Cd(II) complex were investigated in various solvents (e.g., EtOH, MeOH, H_2O, DMF, DMSO, ACN, DCM, acetone, and hexane) as follows: 1 mM solutions of H_2L and Cd(II) complex were prepared in DMF and 2.0 mL of each solvent was added to make the concentration of 20 μM from this stock solution. Then, the suspensions were transferred to quartz cuvettes for experiments. The electronic absorption spectral region was performed by a Shimadzu UV-1800 spectrophotometer. The fluorescence excitation and emission spectra were measured at room temperature using a Varian Eclipse spectrofluorometer with cuvettes having a 1.0-cm path length.

As a result, the maximum absorption wavelength was determined as 365 nm and later, in order to determine the optimum wavelength for excitation in fluorescence analysis, it was decided to use 393 nm as the optimum excitation wavelength as a result of measurements at wavelengths between 360 and 400 nm (Figure 2a). During fluorescence measurements, the ideal concentration was defined as 30×10^{-6} M according to fluorescence calibration (Figure 2b). Stock solutions of each NAC were prepared at a concentration of 1 mM in water, and titration experiments were conducted by gradually adding these stock solutions.

The fluorescence detection capabilities of some NACs (2,4,6-trinitrotoluene (TNT), dinitrobenzene (DNB), 4-nitrophenol (4-NP), 2-nitrophenol (2-NP), 2,4-dinitrotoluene (DNT), 2,4-dinitrophenol (DNP), and 1,3,5-trinitrophenol (TNP)) were examined separately at room temperature. Likewise, measurements were taken with UV–Vis absorption spectra for all NACs (Figure S11). Titration experiments were conducted by incrementally introducing TNT into the system in steps of 0.5 μM. After each addition, the solution was allowed to equilibrate for 1 min. Fluorescence quenching was then observed by monitoring emission at 467 nm following excitation at 393 nm.

3 | Results and Discussion

3.1 | Chemistry

Figures S5 and S6 display the prominent bands and provide evidence of the ligand binding to the metal ion in the complex. H_2L contains characteristic bands at 3426 and 3350, 1668 and 1609, and 1204 and 1188 cm^{-1} due to vibration of υ (OH), υ (HC=N), and υ (Ar-O), respectively (Figure S5). Compared to H_2L, the characteristic bands of the Cd(II) complex are red-shifted, indicating the coordination of the metal ion with the ligand.

In the FTIR spectra of the Cd(II) complex, remarkable changes were observed in the CH=N and phenolic -OH stretching vibrations. When the FTIR spectra of the Cd(II) complex were assessed, it was observed that the phenolic -OH stretching vibration at 3426 and 3350 cm^{-1} in H_2L vanished in the complex compound [31]. In addition, the phenolic C-O stretching vibration seen at 1204 and 1188 cm^{-1} in H_2L showed a shift to the region of 1238 and 1181 cm^{-1} in the Cd(II) complex. These shifts indicate that the phenolic oxygen, which has lost its proton during complex formation, enters into coordination with the metal ion [32].

The CH=N stretching vibration seen at 1668 and 1609 cm^{-1} in H_2L shifted to 1641 and 1618 cm^{-1} in the IR spectra of the Cd(II) complex. This shift indicates that the N atom of the azomethine group is involved in the formation of the M-N

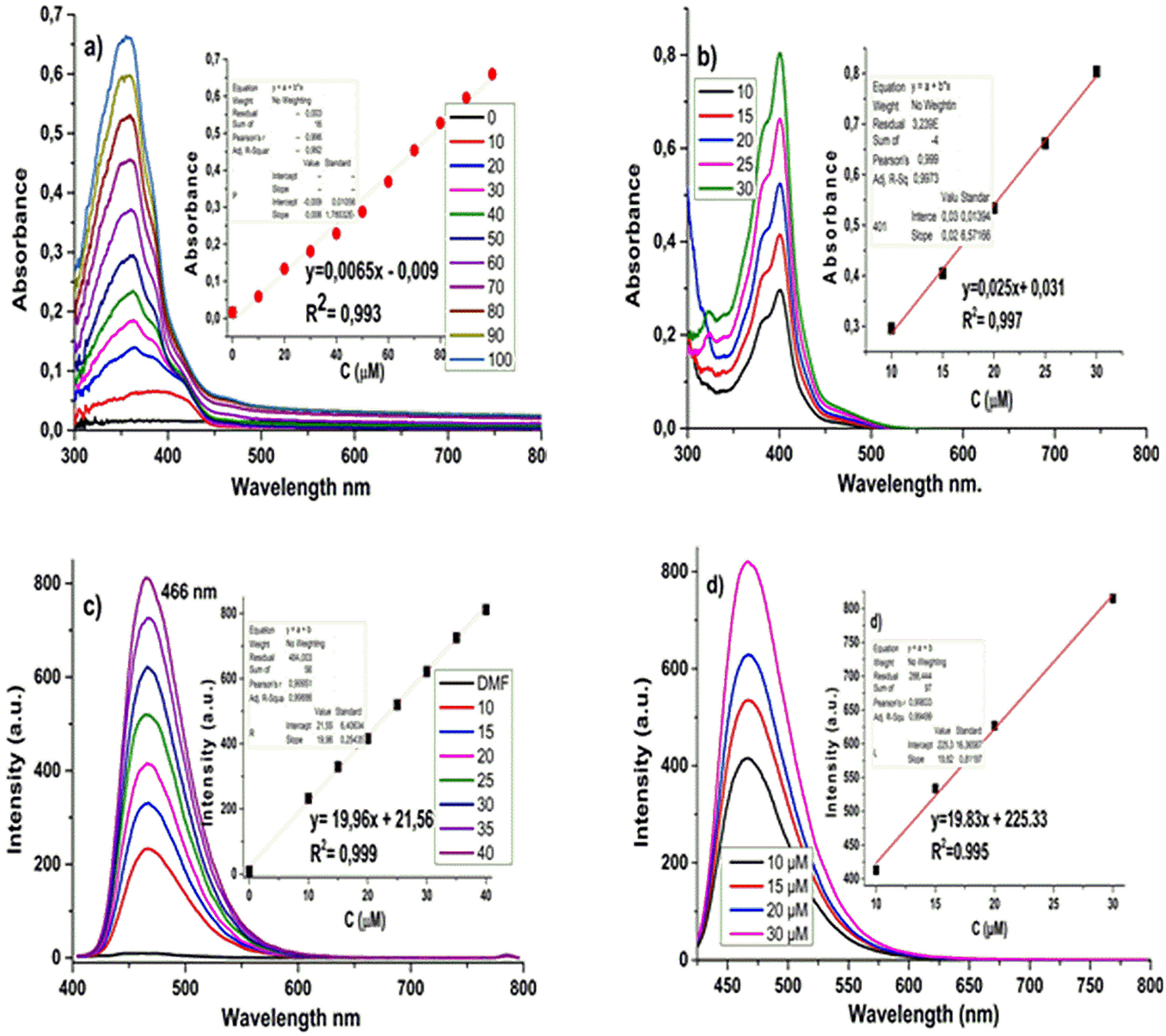

FIGURE 2 | Linear graph by UV–Vis absorption spectra of (a) H_2L and (b) Cd(II) complex and fluorescence spectra of (c) H_2L and (d) Cd(II) complex in DMF ($\lambda_{exc} = 393$ nm and $\lambda_{em} = 467$ nm).

bond [33]. In other words, the nitrogen atom has entered into coordination with the metal by giving its unpaired electrons to the metal ion. The presence of M-N (555–508 cm^{-1}) and M-O (493–461 cm^{-1}) bonds, which are not observed in the Schiff base but observed in the complex, also supports that the coordination takes place through N and O atoms [34]. The C=O and C-S-C stretching vibrations observed at 1689 and 776 cm^{-1} in H_2L did not undergo a significant change in the complex compounds. This indicates that C=O and C-S-C groups do not enter into coordination with metal ions. The diffuse peaks observed at 3418 cm^{-1} in the Cd(II) complex are due to H_2O molecules in the structure (Figure S6). The microanalysis results of the Cd(II) complex showed that a 1:1 complex was formed between the ligand and the metal and 1.5 mol of hydrated water was present in the structure. This is also supported by the results of thermal analysis.

When the ^{1}H-NMR spectra of H_2L was examined, a single peak of one proton belonging to the OH group was observed at 9.48 ppm, a chemical shift observed as a single peak of two protons belonging to the CH=N proton was observed at 8.59 ppm, and multiple peaks belonging to the protons of the aromatic ring were observed at 7.57–6.62 ppm [35, 36]. The peaks observed at $\delta = 3.73$ and 2.74 ppm belong to protons attached to the pyridine ring, and the peak observed at 2.27 ppm belongs to the -CH_3 proton. The integral ratios were found to be compatible with the number of protons in the structure. The ^{13}C-NMR spectra of H_2L showed that the carbons belonging to the azomethine carbon appeared at 162.34 and 159.95 ppm, while the carbons belonging to the aromatic ring and carbonyl group appeared at 157.69–44.99 and 169.78 ppm. The new peaks observed in the FTIR spectra different from the starting material, the absence of NH_2 protons in the ^{1}H-NMR spectra, and

the chemical shift values in the ^{13}C-NMR spectra indicate the formation of Schiff base. In conclusion, the results of infrared, elemental analysis, NMR analysis, and physical properties such as yield, melting point, and color mentioned in the experimental part support the suitability of the proposed structure for the ligand.

^{1}H-NMR spectra of the Cd(II) complex showed that the single peak of OH observed at 9.48 ppm in the ligand disappeared. In addition, the single peak of CH=N observed at 8.59 ppm in the ligand was observed at 8.94 ppm in the Cd(II) complex. This once again supports that the binding to the metal is via azomethine nitrogen and phenol oxygen. The chemical shift values

TABLE 1 | Thermal decomposition of Cd(II) complex.

Complex	Decomp. stages	Temp. range (°C)	Mass loss (%) calcd. (found)		Decomp. assignment
$[H_2LCd(H_2O)_2]1.5H_2O$	1	40–420	29.56	29.42	$3.5H_2O$, 2Br
	2	420–850	38.80	37.07	$C_{19}H_{17}NS$
	Residue	850	31.50	29.16	$C_4N_2O_2 + CdO$

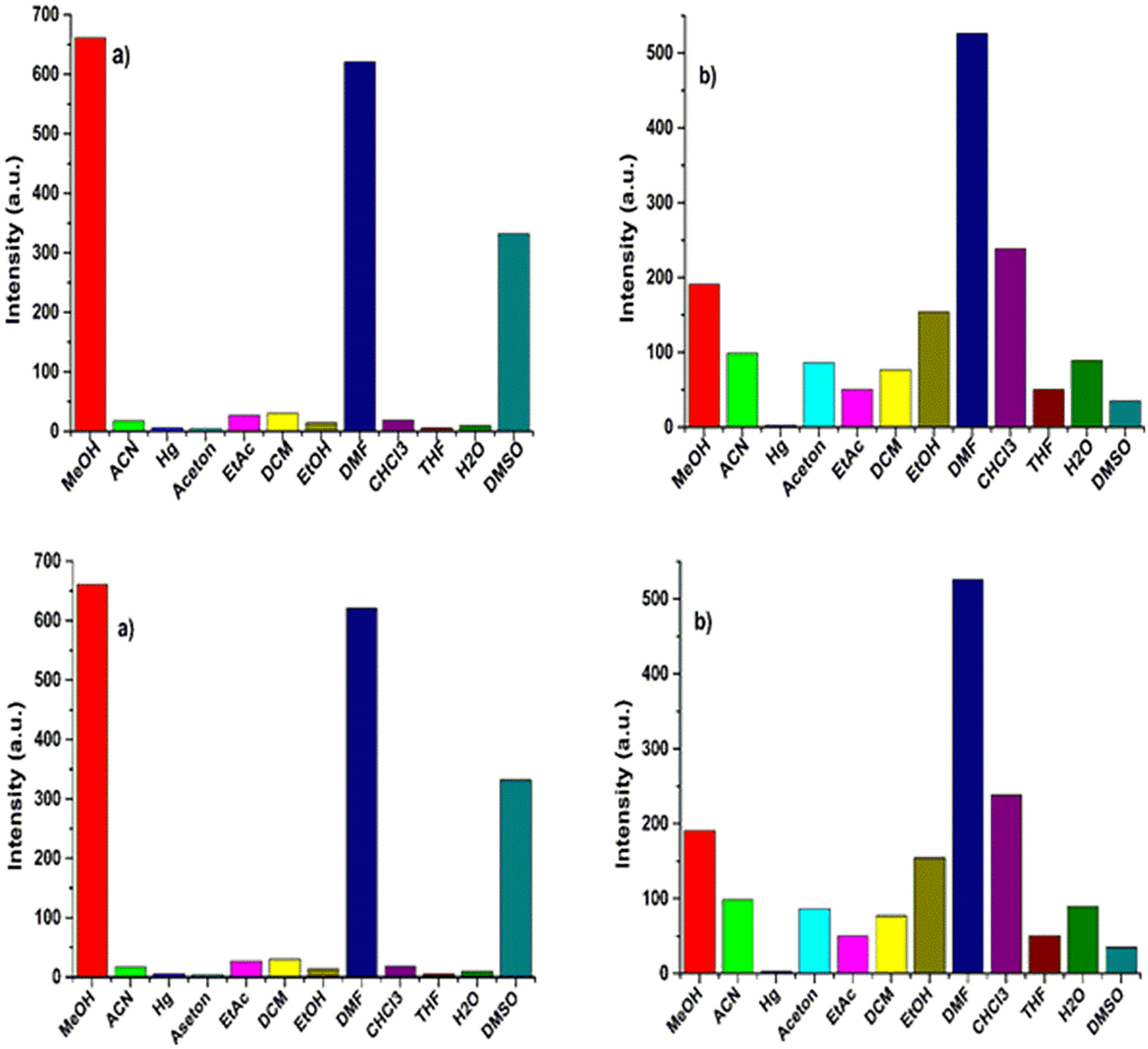

FIGURE 3 | Fluorescence intensity at 467 nm in various solvents of (a) H_2L and (b) Cd(II) complex ($\lambda_{exc} = 393$ nm).

of the other protons showed insignificantly small changes and appeared almost in the same regions as the ligand. In the ^{13}C-NMR spectra of the Cd(II) complex, the azomethine carbon and the carbon atom to which the phenolic OH group is attached are shifted a few ppm to the low field. This supports that these metal ions form chelates with the N atom of the azomethine group and phenolic O atom [37].

The electronic absorption spectra of the Schiff base and metal complex were measured in the range of 200–1100 nm by preparing their solutions in ethanol at a concentration of 10^{-5} M. When the UV–Vis spectra of H_2L were analyzed, peaks due to $\delta \rightarrow \delta^*$, $\pi \rightarrow \pi^*$ in the range 197–285 nm, and $n \rightarrow \pi^*$ transitions in the range 340–395 nm were observed. These peaks are transitions arising from aromatic rings and unpaired electrons (Figure S7). When the electronic spectra of the Cd(II) complex are compared with the spectra of the ligand, some differences are observed. A right shift (red shift) was observed in the complex compound compared to the ligand. When the electronic absorption spectra of the Cd(II) complex are examined, peaks due to $\pi \rightarrow \pi^*$ and $n \rightarrow \pi^*$ transitions are observed at 205–267 and 330–365 nm. The peaks at 410 and 715 nm indicate LMCT transitions (Figure S8) [38]. The magnetic susceptibility measurement of the Cd(II) complex is diamagnetic as expected [39].

TABLE 2 | Analytical parameters of H_2L and Cd(II) complex in DMF.

Analytical parameters	H_2L	Cd(II) complex
ε ($M^{-1}\cdot cm^{-1}$) $\times 10^3$	6.5	25.5
Excitation wavelength (nm)	393	393
Emission wavelength (nm)	467	467
Stokes	50	77
Sensor concentration (μM)	30	20
Linear range (μM)	1–10	1–15
K_{sv} (1/M) $\times 10^3$	111.8	68.3
R^2	0.9923	0.9926
LOD (μM)	0.095	0.257

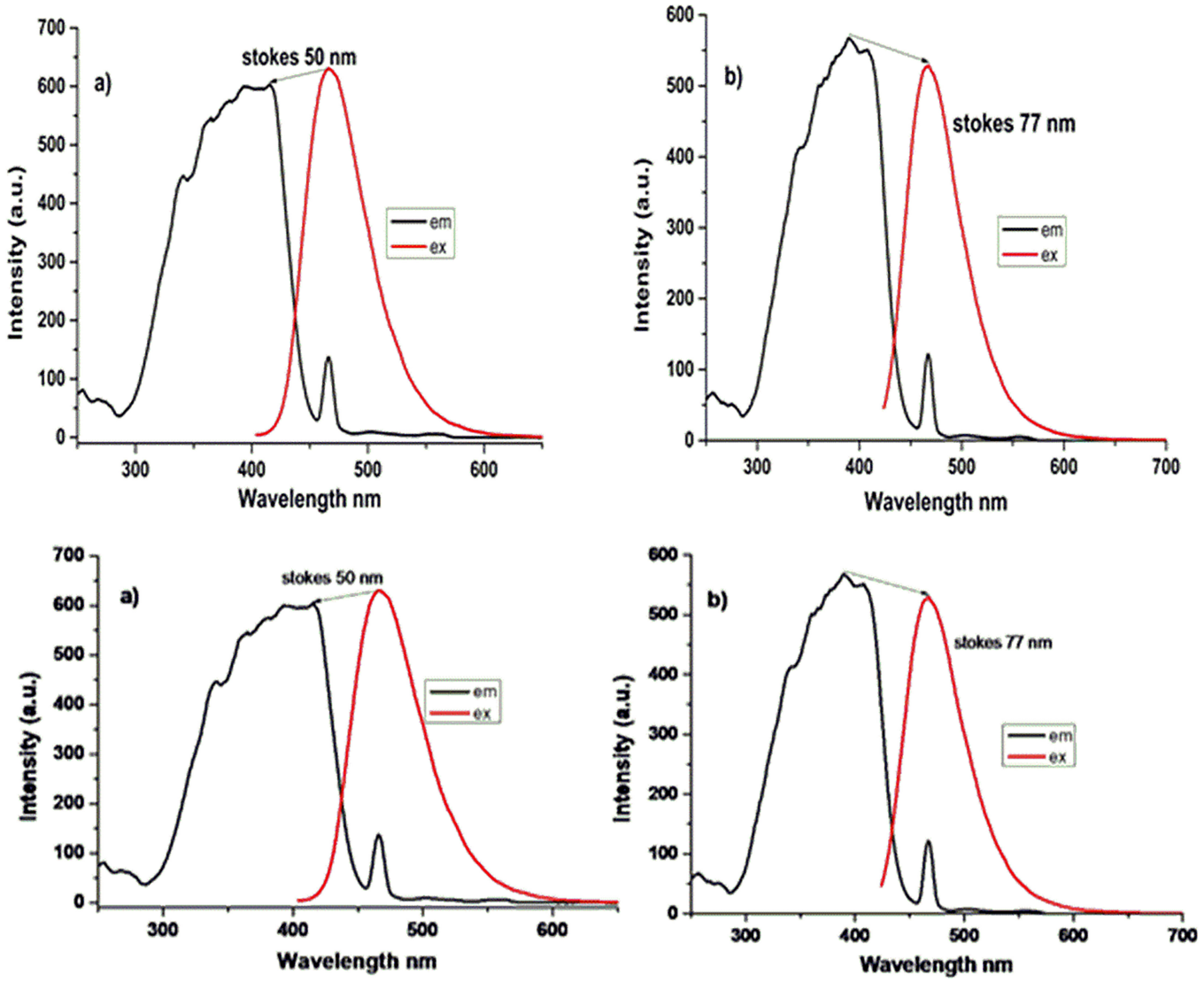

FIGURE 4 | Excitation and emission spectra of (a) H_2L and (b) Cd(II) complex in DMF ($\lambda_{ex} = 393$ nm).

The molecular weight of the Cd(II) complex is in agreement with the molecular ion mass. This value confirms the structure of the complex, that is, proves that the synthesis has taken place [40]. In the mass spectra of the Cd(II) complex, the main peak was observed at 752.226 corresponding to the $[M\text{-}2H]^+$ molecular ion (Figure S9).

3.2 | Thermal Studies (TGA-DTA)

Thermogravimetric measurements were used to study the thermal behavior of the combined compound over a temperature range of 25°C–800°C. The TG curve of the Cd(II) complex displays two decomposition steps (Table 1). The loss of 1.5 mol hydrated H_2O, two coordinated H_2O, and two moles Br occurs during the first breakdown step, which occurs between 40°C and 420°C; this is read as a weight loss of (found/calc. %; 29.42 (29.56)). The breakdown of the $C_{19}H_{17}NS$ moiety takes place in the second step, which is between 420°C and 850°C; the anticipated weight loss range for this phase is (found/calc. %; 37.07 (38.80)). The mass decrease in the last step is thought to represent the full breakdown of the $C_4N_2O_2$ moiety, leaving CdO as the final residue (Figure S10).

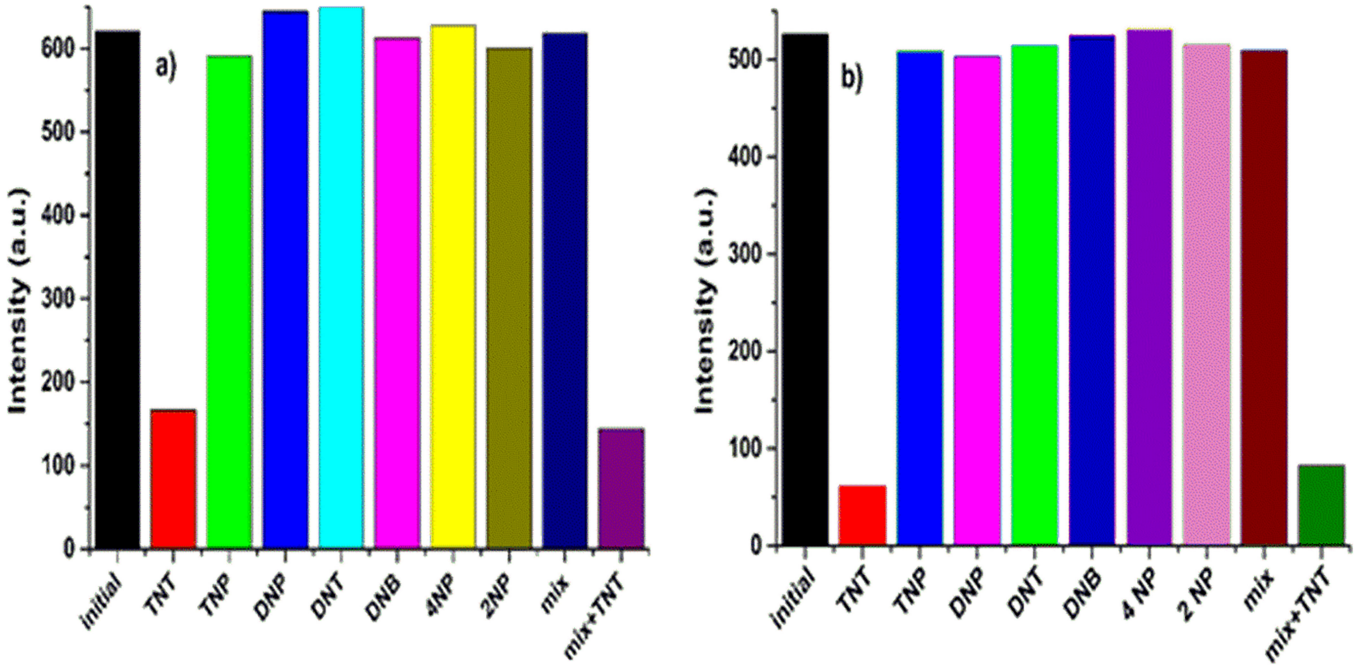

FIGURE 5 | Fluorescence intensity at 467 nm upon addition of different NACs of (a) H_2L and (b) Cd(II) complex in DMF ($\lambda_{exc} = 393$ nm).

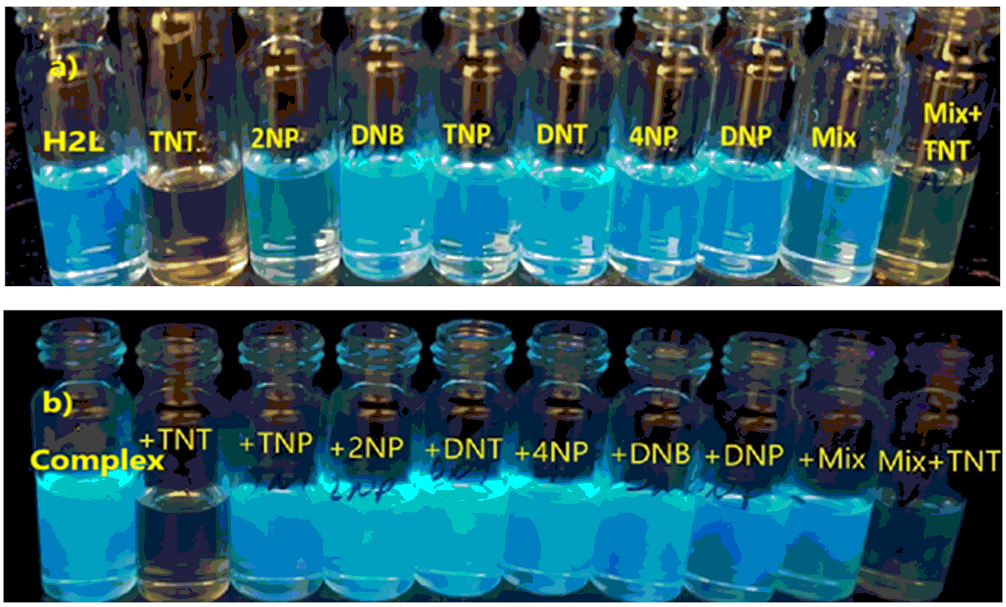

FIGURE 6 | Photograph under 365-nm UV lamp of fluorescence color changes of (a) H_2L and (b) Cd(II) complex upon addition of three equivalents of different NACs.

3.3 | Photophysical Properties

The absorption and fluorescence spectra of sensors Schiff base and its Cd(II) complex (20 μM) were measured in various solvents including water, THF, methanol, ethanol, ACN, DMF, acetone, EtAc, DCM, $CHCl_3$, and hexane to evaluate the effect of solvents on absorption and emission properties (Figure S12). When fluorescence measurements of H_2L were performed in different solvents, the best results were obtained in methanol (Figure 3a). However, since the fluorescence property of H_2L in methanol was unstable, it was decided to work in the DMF solution with the second highest intensity. For the complex, the experiment was performed in the DMF solution with the highest intensity (Figure 3b).

H_2L and Cd(II) complex exhibited strong absorption bands at 365 nm ($\varepsilon = 6.5 \times 10^3\ M^{-1}\ cm^{-1}$) and 401 nm ($\varepsilon = 20 \times 10^6\ M^{-1}\ cm^{-1}$) (Figure 2a,c), and their molar extinction coefficients were found to be higher than many previously reported systems. Upon excitation at 393 nm, both H_2L and Cd(II) complex showed fluorescence emissions centered at 467 nm in DMF (Figure 2b,d). Study concentrations were fixed at 30 μM for H_2L and 20 μM for Cd(II) complex. The Stokes shift of H_2L and Cd(II) complex was determined as 50 and 70 nm in DMF, respectively (Figure 4). Analytical parameters of H_2L and Cd(II) complex are given in Table 2.

The fluorescence emission spectra of compounds remained almost unchanged by the addition of NACs (DNT, DNP, DNB, TNP, 4-NP, 2-NP) solutions separately, except for TNT (Figures 5 and 6). The fluorescence intensity of Cd(II) complex was effectively quenched by the addition of TNT. The fluorescence intensity of H_2L and Cd(II) complex at 467 nm decreased by approximately 73.4% and 88.2%, respectively, in the presence of TNT. The

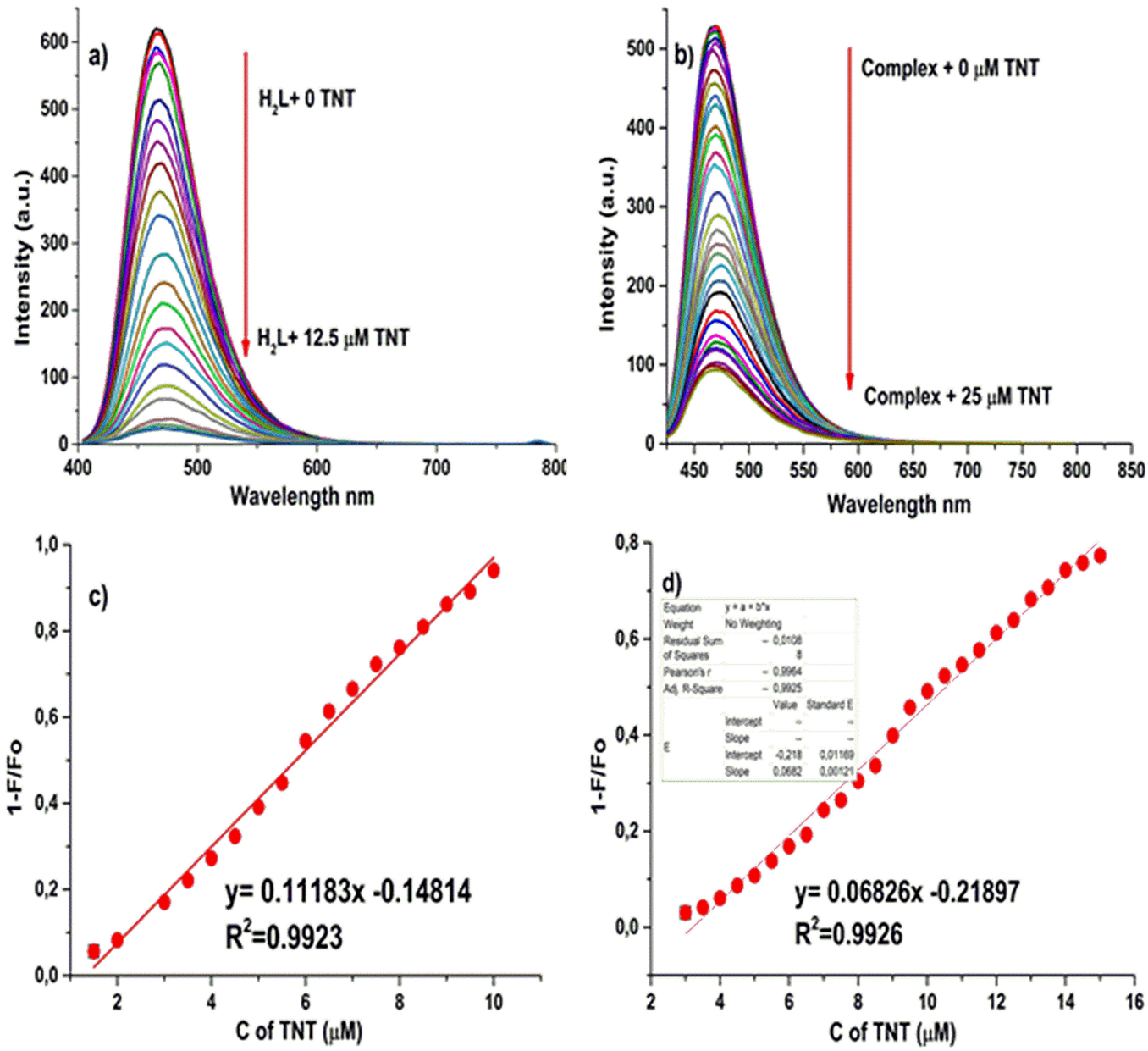

FIGURE 7 | Fluorescence titration spectra of (a) H_2L and (b) Cd(II) complex, Stern–Volmer linear graph of (c) H_2L and (d) Cd(II) complex upon incremental addition of TNT in solution medium ($\lambda_{exc} = 393$ nm and $\lambda_{em} = 467$ nm).

compounds used in this study have been shown to selectively interact with TNT through intermolecular π-π and CH-π stacking interactions, resulting in an effective electron transfer resulting in a "turn-off" response.

The negative charge on the methyl anion is distributed throughout the TNT molecule through resonance stabilization by the three electron-withdrawing nitro groups. The anionic form of TNT can strongly absorb visible light, which can lead to a change in solution color [41].

As shown in Figure 6, when TNT was added, the fluorescence intensity at 467 nm gradually decreased and probes H_2L and Cd(II) complex showed visual color change from blue to colorless under a 365-nm UV lamp when TNT was added. Moreover, there was a good linear relationship between the maximum fluorescence intensity of H_2L and Cd(II) complex and the TNT concentration changing up to 1–10 and 1–15 μM, respectively (Figure 7). These materials show significant fluorescence quenching against TNT with a high Stern–Volmer constant (K_{sv}) of $111.8 \times 10^3\ M^{-1}$ for H_2L and $68.3 \times 10^3\ M^{-1}$ for Cd(II) complex.

The limit of detection (LOD) of H_2L and Cd(II) complex for TNT was determined using the equation $3\sigma / k$, where σ is the standard deviation of blank measurements and k is the slope of the calibration curve. When calculated according to the fluorescence titration curve values, it is seen that the LOD value of H_2L is 0.095, which is lower than the LOD value of Cd(II) complex (0.257 mM). Also, the LOD value of H2L is 0.095 mM, which is better than the values in the literature [12, 19, 42–45].

The fluorescence signals of both the H_2L and Cd(II) complex without and in the presence of TNT are observed to change by less than 10% over a 100-min period. This observation highlights the remarkable photostability of the materials, emphasizing their resistance to degradation upon prolonged exposure to light (Figure 8).

The stoichiometric relationship of H_2L and Cd(II) complex with TNT was examined with Job's graph. For this purpose, TNT mole fractions were added to H_2L and Cd(II) complex (40 μM) at the same molar ratio, and fluorescence measurements were taken. Figure 9 shows that the minimum fluorescence signal for H_2L and Cd(II) complex was displayed at 0.3 and 0.4 mol TNT fractions, respectively. Job graphs in TNT fraction show that there is a 2:1 and 2:3 binding stoichiometry between H_2L and Cd(II) complex with TNT, respectively.

In this work, the fluorescence lifetimes of H_2L and H_2L+TNT were measured under optimized conditions, yielding values of 1.270 ± 0.004 (τ_0) and 3.420 ± 0.021 (τ), respectively (Figure 10a).

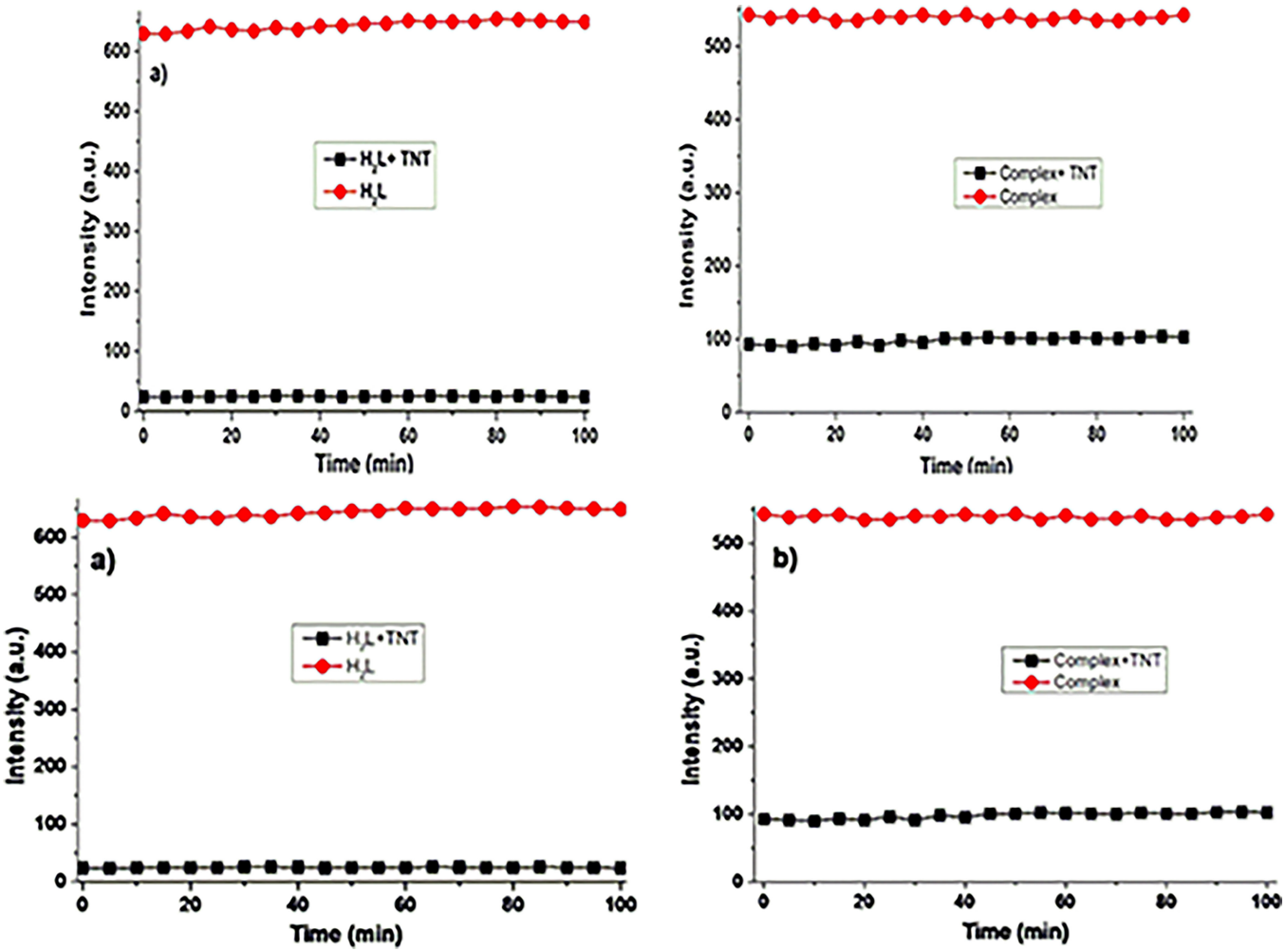

FIGURE 8 | Fluorescence photostability of (a) H_2L and H_2L+TNT and (b) Cd(II) complex and Cd(II) complex+TNT ($\lambda_{exc} = 393$ nm and $\lambda_{em} = 467$ nm).

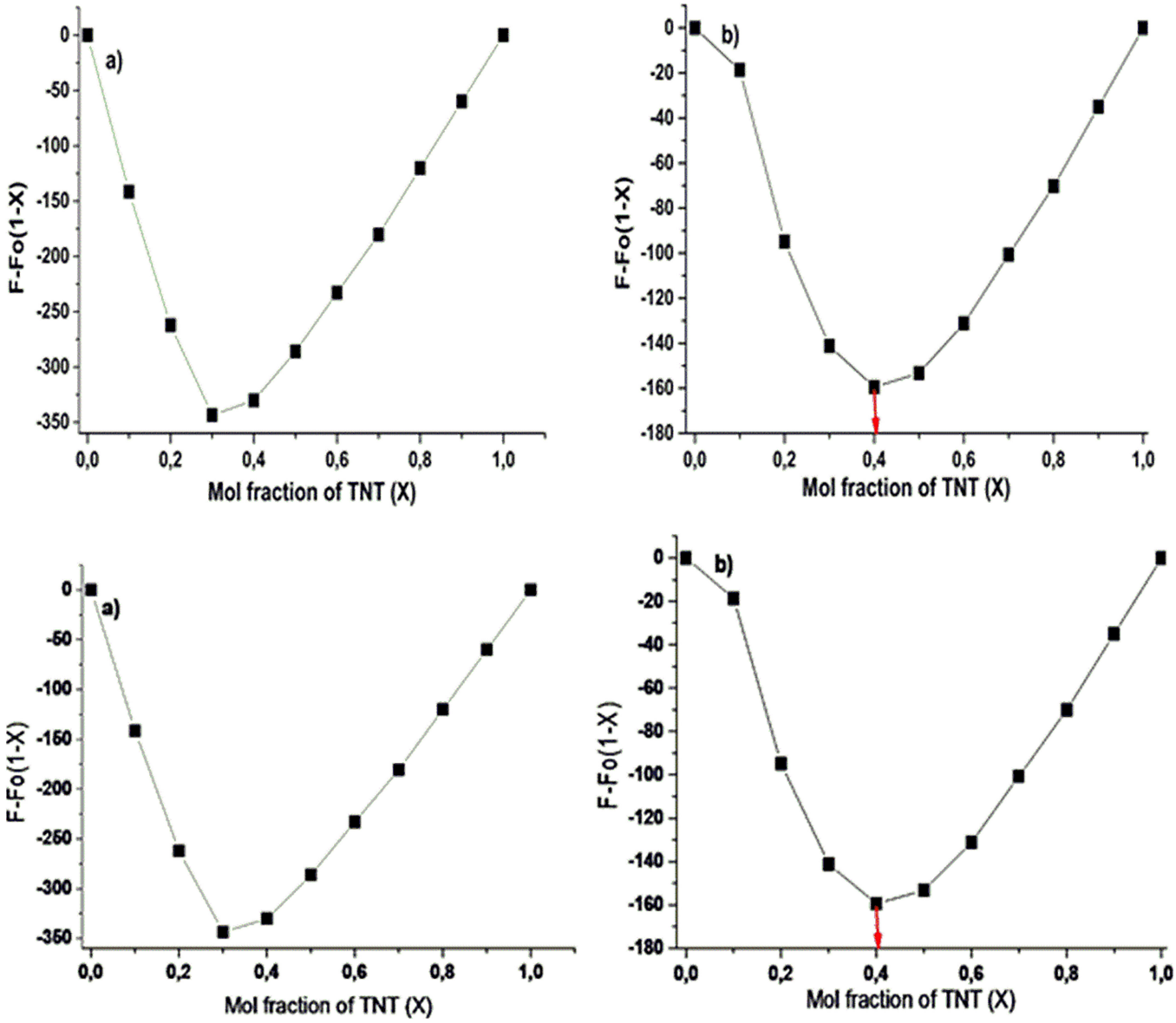

FIGURE 9 | Job's plot graph of (a) H_2L and (b) Cd(II) complex with TNT.

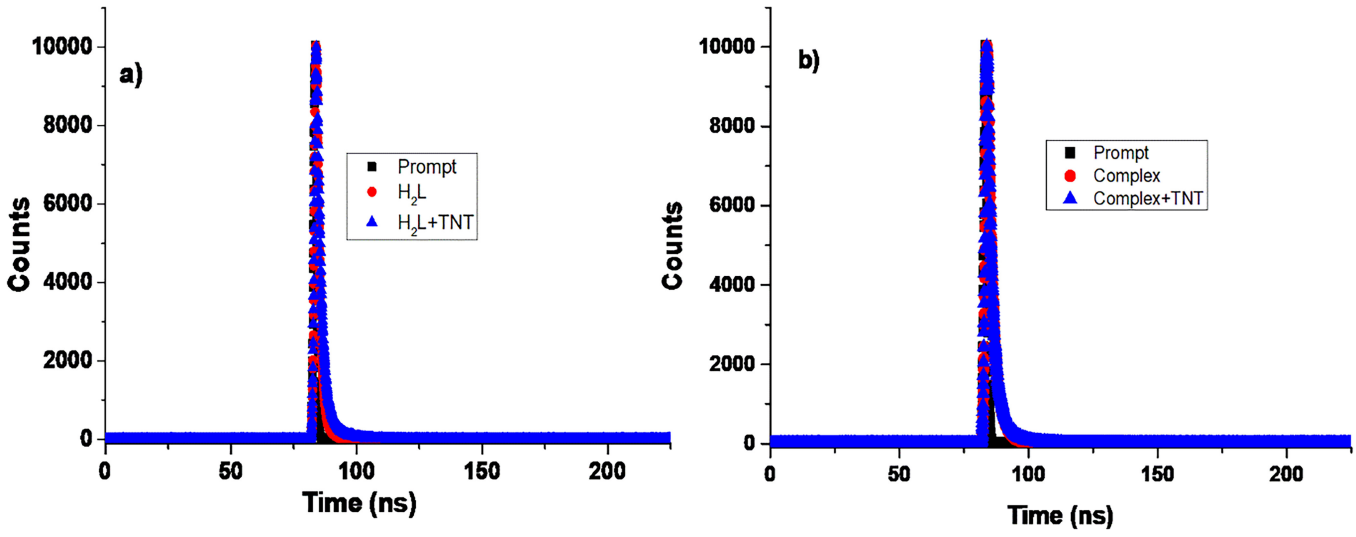

FIGURE 10 | Fluorescence lifetimes of (a) H_2L, H_2L + TNT and (b) Cd(II) complex, Cd(II) complex + TNT in DMF with 390-nm laser excitation source.

Furthermore, the fluorescence lifetimes for the Cd(II) complex and the Cd(II) complex + TNT were performed under optimized conditions, yielding values of 2.810 ± 0.021 (τ_0) and 3.995 ± 0.025 (τ) (Figure 10b). These experimental results confirmed that the fluorescence quenching response of compounds was primarily due to the formation of a nonfluorescent complex [46].

4 | Conclusion

The Schiff base (H_2L) and its Cd(II) complex were successfully synthesized. The identities of all synthesized compounds were verified using a combination of ^{1}H-NMR, ^{13}C-NMR, FTIR, mass, microanalysis, UV–Vis, magnetic susceptibility, and thermogravimetric analysis. The analytical data indicated that the reaction between H_2L and the Cd(II) cation resulted in the formation of the binuclear complex with a 1:1 M ratio of ligand to metal. The synthesized compounds exhibited remarkable sensor capabilities against various NACs. H_2L was found to have excellent sensitivity against TNT with a low LOD value (0.095 μM) and a high Stern–Volmer constant (K_{sv}: $111.8 \times 10^3\,M^{-1}$) in the linear range of 1–10 μM. The compounds showed good fluorescence properties, and it was concluded that they could be good sensors for fluorescence quenching–based TNT detection. In particular, H_2L showed both high selectivity and sensitivity in detecting TNT. Fluorescence signals of both the ligand and the complex without and in the presence of TNT are seen to be photostable for 100 min. Consequently, the targeted compounds emerge as a promising candidate to serve as a specifically designed sensor for the detection of NACs.

Author Contributions

N.T: investigation, writing – original draft, methodology, validation, visualization, writing – review and editing, project administration, supervision, resources. **A.A:** investigation, writing – original draft, supervision, resources, visualization, validation, methodology, writing – review and editing. **K.B:** visualization, validation, supervision. **O.A:** investigation, validation, visualization, methodology, supervision, resources. All authors read and approved the final manuscript.

Acknowledgments

This research was supported by the Muş Alparslan University Scientific Research Project Unit under project number BAP-22-FEF-4902-08.

Conflicts of Interest

The authors declare no conflicts of interest.

Data Availability Statement

The data that support the findings of this study are available from the corresponding authors upon reasonable request.

References

1. M. Kumar, A. K. Singh, A. K. Singh, et al., "Recent Advances in 3d-Block Metal Complexes With Bi, Tri, and Tetradentate Schiff Base Ligands Derived From Salicylaldehyde and Its Derivatives: Synthesis, Characterization and Applications," *Coordination Chemistry Reviews* 488 (2023): 215176, https://doi.org/10.1016/j.ccr.2023.215176.

2. A. Altun, K. Buldurun, and N. Turan, "Enhanced Luminescent Probe Utilizing Schiff Base Ligand for 2,4,6-Trinitrophenol Detection in Aqueous Media," *Journal of the Institute of Science and Technology* 15 (2025): 228–240, https://doi.org/10.21597/jist.1540673.

3. Y. Zhang, Y.-X. Su, Z. Cai, L. Tong, and W.-K. Dong, "Structural, Fluorescent and Theoretical Studies of a More Flexible Salamo-Type Ligand and Its Uncommon Tetranuclear Chloride-Bridged Nickel (II) Complex," *Journal of Molecular Structure* 1309 (2024): 138164, https://doi.org/10.1016/j.molstruc.2024.138164.

4. G. Singh, D. S. Tamana, H. Mithun, et al., "Luminescent Schiff Base Derived Triazolyl Silane: An Emerging Sensor for Detection of Fe^{3+}, Cu^{2+} and a Ceruloplasmin Inducer Validated via Docking," *Journal of Photochemistry and Photobiology A: Chemistry* 448 (2024): 115329, https://doi.org/10.1016/j.jphotochem.2023.115329.

5. D. Ejarque, T. Calvet, M. Font-Bardia, and J. Pons, "Structural Influence of the Length and Functionality of N,N-Donor Spacers in Cd (II) Ladder-Type Coordination Polymers," *Journal of Molecular Structure* 1277 (2023): 134896, https://doi.org/10.1016/j.molstruc.2022.134896.

6. A. A. Mohamed, F. M. Ahmed, W. A. Zordok, W. H. El-Shwiniy, S. A. Sadeek, and H. S. Elshafie, "Novel Enrofloxacin Schiff Base Metal Complexes: Synthesis, Spectroscopic Characterization, Computational Simulation and Antimicrobial Investigation Against Some Food and Phyto-Pathogens," *Inorganics* 10 (2022): 177, https://doi.org/10.3390/inorganics10110177.

7. M. N. Uddin, S. S. Ahmed, and S. M. R. Alam, "Review: Biomedical Applications of Schiff Base Metal Complexes," *Journal of Coordination Chemistry* 73 (2020): 3109–3149, https://doi.org/10.1080/00958972.2020.1854745.

8. P. Sen, D. Akagunduz, A. S. Aghdam, F. Ç. Cebeci, T. Nyokong, and T. Catal, "Synthesis of Novel Schiff Base Cobalt (II) and Iron (III) Complexes as Cathode Catalysts for Microbial Fuel Cell Applications," *Journal of Inorganic and Organometallic Polymers and Materials* 30 (2020): 1110–1120, https://doi.org/10.1007/s10904-019-01286-x.

9. A. Z. El-Sonbati, M. A. Diab, S. M. Morgan, M. I. Abou-Dobara, and A. A. El-Ghettany, "Synthesis, Characterization, Theoretical and Molecular Docking Studies of Mixed Ligand Complexes of Cu (II), Ni (II), Co (II), Mn (II), Cr (III), UO_2(II) and Cd (II)," *Journal of Molecular Structure* 1200 (2020): 127065, https://doi.org/10.1016/j.molstruc.2019.127065.

10. N. R. Divyashree, H. D. Revanasiddappa, N. R. Bhavya, et al., "Azaneylylidene-Based Tetradentate Schiff Base as a New "ON-OFF" Fluorescent Probe for the Detection of Cu (II) Ion: Synthesis, Characterization and Real Sample Analysis," *Spectrochimica Acta, Part A: Molecular and Biomolecular Spectroscopy* 292 (2023): 122435, https://doi.org/10.1016/j.saa.2023.122435.

11. C. Qi, H. Liu, J. Lyu, H. Zhao, and Z.-Y. Lu, "Anthracene and Porphyrin-Based Conjugated Microporous Polymer for Nitrofuran Antibiotics and Nitroaromatic Explosives Detection," *Journal of Environmental Chemical Engineering* 11 (2023): 111553, https://doi.org/10.1016/j.jece.2023.111553.

12. X. Sun, Y. Wang, and Y. Lei, "Fluorescence Based Explosive Detection: From Mechanisms to Sensory Materials," *Chemical Society Reviews* 44 (2015): 8019–8061, https://doi.org/10.1039/C5CS00496A.

13. C. Zhu, H. Huang, and Y. Chen, "Recent Advances in Biological Removal of Nitroaromatics From Wastewater," *Environmental Pollution* 307 (2022): 119570, https://doi.org/10.1016/j.envpol.2022.119570.

14. T. Huang, G. Sun, L. Zhao, N. Zhang, R. Zhong, and Y. Peng, "Quantitative Structure-Activity Relationship (QSAR) Studies on the Toxic Effects of Nitroaromatic Compounds (NACs): A Systematic Review," *International Journal of Molecular Sciences* 22 (2021): 8557, https://doi.org/10.3390/ijms22168557.

15. S. Rathi, P. S. Kumar, and D.-V. N. Vo, "Critical Review on Hazardous Pollutants in Water Environment: Occurrence, Monitoring, Fate, Removal Technologies and Risk Assessment," *Science of the Total Environment* 797 (2021): 149134, https://doi.org/10.1016/j.scitotenv.2021.149134.

16. R. Sinha, N. Roy, R. Rajasekhar, A. Karnawat, and T. K. Mandal, "N-Doped Carbon Dot From Cigarette-Tobacco: Picric Acid Sensing in Real Water Sample and Synthesis of CD-MWCNT Nano-Composite for UV-Photodetection," *Journal of Environmental Chemical Engineering* 9 (2021): 104971, https://doi.org/10.1016/j.jece.2020.104971.

17. G. Sathiyan, G. Venkatesan, S. K. Ramasamy, J. Lee, and S. Barathi, "Recent Progress in Triazine-Based Fluorescent Probes for Detecting Hazardous Nitroaromatic Compounds," *Journal of Environmental Chemical Engineering* 12 (2024): 112804, https://doi.org/10.1016/j.jece.2024.112804.

18. M. T. Montgomery, R. B. Coffin, T. J. Boyd, J. P. Smith, S. E. Walker, and C. L. Osburn, "2,4,6-Trinitrotoluene Mineralization and Bacterial Production Rates of Natural Microbial Assemblages From Coastal Sediments," *Environmental Pollution* 159 (2011): 3673–3680, https://doi.org/10.1016/j.envpol.2011.07.018.

19. S. O. Tümay and S. Yeşilot, "Small Molecule Based Water-Soluble Fluorescence Material for Highly Selective and Ultra-Sensitive Detection of TNT: Design and Spectrofluorimetric Determination in Real Samples," *Sensors and Actuators B: Chemical* 343 (2021): 130088, https://doi.org/10.1016/j.snb.2021.130088.

20. T. P. Forbes and E. Sisco, "Recent Advances in Ambient Mass Spectrometry of Trace Explosives," *Analyst* 143 (2018): 1948–1969, https://doi.org/10.1039/C7AN02066J.

21. J. S. Caygill, F. Davis, and S. P. J. Higson, "Current Trends in Explosive Detection Techniques," *Talanta* 88 (2012): 14–29, https://doi.org/10.1016/j.talanta.2011.11.043.

22. J. W. Grate, R. G. Ewing, and D. A. Atkinson, "Vapor-Generation Methods for Explosives-Detection Research," *TrAC Trends in Analytical Chemistry* 41 (2012): 1–14, https://doi.org/10.1016/j.trac.2012.08.007.

23. J. N. Malegaonkar, M. Al Kobaisi, P. K. Singh, S. V. Bhosale, and S. V. Bhosale, "Sensitive Turn-Off Detection of Nitroaromatics Using Fluorescent Tetraphenylethylene Phosphonate Derivative," *Journal of Photochemistry and Photobiology A: Chemistry* 438 (2023): 114530, https://doi.org/10.1016/j.jphotochem.2022.114530.

24. C. P. Wang, W. W. Sheng, C. Sun, J. Lei, and J. S. Hu, "A Cobalt-Coordination Polymer as a Highly Selective and Sensitive Luminescent Sensor for Detecting 2,4,6-Trinitrophenol," *Journal of Molecular Liquids* 768 (2024): 117–126, https://doi.org/10.1080/15421406.2023.2262857.

25. Y. Salinas, R. Martínez-Máñez, M. D. Marcos, et al., "Optical Chemosensors and Reagents to Detect Explosives," *Chemical Society Reviews* 41 (2012): 1261–1296, https://doi.org/10.1039/C1CS15173H.

26. H. A. Yu, D. A. DeTata, S. W. Lewis, and D. S. Silvester, "Recent Developments in the Electrochemical Detection of Explosives: Towards Field-Deployable Devices for Forensic Science," *TrAC Trends in Analytical Chemistry* 97 (2017): 374–384, https://doi.org/10.1016/j.trac.2017.10.007.

27. M. Calcerrada, M. González-Herráez, and C. García-Ruiz, "Recent Advances in Capillary Electrophoresis Instrumentation for the Analysis of Explosives," *TrAC Trends in Analytical Chemistry* 75 (2016): 75–85, https://doi.org/10.1016/j.trac.2015.08.005.

28. V. Desai, K. Modi, F. Panjwani, et al., "Design and Synthesis of an Efficient Fluorescent Probe Based on Oxacalix[4]arene for the Selective Detection of Trinitrophenol (TNP) Explosives in Aqueous System," *Journal of Fluorescence* 34 (2024): 1219–1228, https://doi.org/10.1007/s10895-023-03352-7.

29. K. J. Wang, R.-H. Gao, Y. Fan, C. Huang, B.-X. Zhu, and J.-H. Lu, "Synthesis, Crystal Structures, and Alcohol Vapor Adsorption Properties of Cd (II) and Cu (II) Complexes Based on a Salen-Type Schiff Base," *Inorganica Chimica Acta* 571 (2024): 122208, https://doi.org/10.1016/j.ica.2024.122208.

30. O. Aydın, Master Thesis, Natural and Applied Science, Muş Alparslan University, Muş/Turkey (2024).

31. Z. Beigi, A. H. Kianfar, H. Farrokhpour, M. Roushani, M. H. Azarian, and W. A. K. Mahmood, "Synthesis, Characterization and Spectroscopic Studies of Nickel (II) Complexes With Some Tridentate ONN Donor Schiff Bases and Their Electrocatalytic Application for Oxidation of Methanol," *Journal of Molecular Liquids* 249 (2018): 117–125, https://doi.org/10.1016/j.molliq.2017.10.131.

32. V. K. Bhovi, K. Bharathi, S. P. Melinmath, V. Basavanna, and S. Ningaiah, "Transition Metal (II) Complexes of (*E*)-N-(4-Methylbenzylidene)-2-((*Z*)-(4-Methylbenzylidene)amino)benzamides: Synthesis, Characterization and Their Biological Evaluation," *Biointerface Research in Applied Chemistry* 12, no. 3 (2022): 3607–3617, https://doi.org/10.33263/BRIAC123.36073617.

33. H. F. Abd El-Halim, M. M. Omar, G. G. Mohamed, and M. A. El-Ela Sayed, "Spectroscopic and Biological Activity Studies on Tridentate Schiff Base Ligands and Their Transition Metal Complexes," *European Journal of Chemistry* 2 (2011): 178–188, https://doi.org/10.5155/eurjchem.2.2.178-188.240.

34. Y. B. Zemede, D. Nithyakalyani, and S. A. Kumar, "Synthesis, Characterization and Antimicrobial Properties of Some Transition Metal Complexes With NS-Chelating Schiff Base Ligand Incorporating Thiophene and Sulfonamide Moieties," *Asian Journal of Chemistry* 27 (2015): 941–948, https://doi.org/10.14233/ajchem.2015.17627.

35. G. Ceyhan, C. Çelik, S. Urus, İ. Demirtas, M. Elmastas, and M. Tümer, "Antioxidant, Electrochemical, Thermal, Antimicrobial and Alkane Oxidation Properties of Tridentate Schiff Base Ligands and Their Metal Complexes," *Spectrochimica Acta Part A: Molecular Spectroscopy* 81 (2011): 184–198, https://doi.org/10.1016/j.saa.2011.05.106.

36. N. Turan, E. Tanış, K. Buldurun, and N. Çolak, "Synthesis, Structure, DFT Calculations, and in Silico Toxic Potential of Ni (II), Zn (II), and Fe (II) Complexes With a Tridentate Schiff Base," *Russian Journal of General Chemistry* 91, no. 8 (2021): 1572–1577, https://doi.org/10.1134/S107036322108020X.

37. M. Bingöl and N. Turan, "Schiff Base and Metal (II) Complexes Containing Thiophene-3-Carboxylate: Synthesis, Characterization and Antioxidant Activities," *Journal of Molecular Structure* 1205 (2020): 127542, https://doi.org/10.1016/j.molstruc.2019.127542.

38. H. A. M. Bennour, F. M. Elmagbari, A. N. Hammouda, et al., "Synthesis, Characterisation and Density Functional Theory (DPT) Studies of a Triazine Ring With a Mixed Ligand Schiff Base Complexes," *Research Chemicals* 5 (2023): 100775, https://doi.org/10.1016/j.rechem.2023.100775.

39. M. M. E. Shakdofa, H. A. Mousa, A. A. Labib, A. S. Abd-El-Ali, A. A. El-Beih, and M. M. Abdalla, "Synthesis and Characterization of Novel Chromone Schiff Base Complexes as p53 Activators," *Applied Organometallic Chemistry* 32, no. 6 (2018): e4345, https://doi.org/10.1002/aoc.4345.

40. N. Turan, K. Buldurun, F. Türkan, et al., "Some Metal Chelates With Schiff Base Ligand: Synthesis, Structure Elucidation, Thermal Behavior, XRD Evaluation, Antioxidant Activity, Enzyme Inhibition, and Molecular Docking Studies," *Molecular Diversity* 26 (2022): 2459–2472, https://doi.org/10.1007/s11030-021-10344-x.

41. R. Tu, B. Liu, Z. Wang, et al., "Amine-Capped ZnS-Mn^{2+} Nanocrystals for Fluorescence Detection of Trace TNT Explosive," *Analytical Chemistry* 80 (2008): 3458–3465, https://doi.org/10.1021/ac800060f.

42. L. Fan, Y. Hu, X. Wang, et al., "Fluorescence Resonance Energy Transfer Quenching at the Surface of Graphene Quantum Dots for Ultrasensitive Detection of TNT," *Talanta* 101 (2012): 192–197, https://doi.org/10.1016/j.talanta.2012.08.048.

43. S. Xu, H. Lu, J. Li, et al., "Dummy Molecularly Imprinted Polymers-Capped CdTe Quantum Dots for the Fluorescent Sensing of 2,4,6-Trinitrotoluene," *ACS Applied Materials & Interfaces* 5 (2013): 8146–8154, https://doi.org/10.1021/am4022076.

44. J.-H. Hong, J.-H. Choi, and D.-G. Cho, "Simple Pyrene Derivatives as Fluorescence Sensors for TNT and RDX in Micelles," *Bulletin of the Korean Chemical Society* 35 (2014): 3158–3162, https://doi.org/10.5012/BKCS.2014.35.11.3158.

45. H. Nie, Y. Lv, L. Yao, et al., "Fluorescence Detection of Trace TNT by Novel Cross-Linking Electropolymerized Films Both in Vapor and Aqueous Medium," *Journal of Hazardous Materials* 264 (2014): 474–480, https://doi.org/10.1016/j.jhazmat.2013.09.031.

46. A. Altun, "Utilization of Schiff Base-Co (II) Complex as a Stable Luminescent Probe for the Highly Selective Detection of 2,4,6-Trinitrophenol in an Aqueous Medium," *Journal of Luminescence* 271 (2024): 120593, https://doi.org/10.1016/j.jlumin.2024.120593.

Supporting Information

Additional supporting information can be found online in the Supporting Information section.